Homology Modeling of Rat and Human Cytochrome P450 2D (CYP2D) Isoforms and Computational Rationalization of Experimental Ligand-Binding Specificities

Jennifer Venhorst,[†] Antonius M. ter Laak,[†] Jan N. M. Commandeur,[†] Yoshihiko Funae,[‡] Toyoko Hiroi,[‡] and Nico P. E. Vermeulen*[,†]

Department of Pharmacochemistry, Faculty of Sciences, Division of Molecular Toxicology, Leiden/Amsterdam Center for Drug Research (LACDR), Vrije Universiteit, De Boelelaan 1083, 1081 HV Amsterdam, The Netherlands, and Laboratory of Chemistry, Osaka University Medical School, 1-4-54, Asahimachi, Abeno-ku, Osaka 545, Japan

Received June 10, 2002

The ligand-binding characteristics of rat and human CYP2D isoforms, i.e., rat CYP2D1−4 and human CYP2D6, were investigated by measuring IC_{50} values of 11 known CYP2D6 ligands using 7-methoxy-4-(aminomethyl)coumarin (MAMC) as substrate. Like CYP2D6, all rat CYP2D isozymes catalyzed the O-demethylation of MAMC with K_m and V_{max} values ranging between 78 and 145 μM and 0.048 and 1.122 min^{-1}, respectively. To rationalize observed differences in the experimentally determined IC_{50} values, homology models of the CYP2D isoforms were constructed. A homology model of CYP2D6 was generated on the basis of crystallized rabbit CYP2C5 and was validated on its ability to reproduce binding orientations corresponding to metabolic profiles of the substrates and to remain stable during unrestrained molecular dynamics simulations at 300 K. Twenty-two active site residues, sharing up to 59% sequence identity, were identified in the CYP2D binding pockets and included CYP2D6 residues Phe120, Glu216, and Asp301. Electrostatic potential calculations displayed large differences in the negative charge of the CYP2D active sites, which was consistent with observed differences in absolute IC_{50} values. MD studies on the binding mode of sparteine, quinidine, and quinine in CYP2D2 and CYP2D6 furthermore concurred well with experimentally determined IC_{50} values and metabolic profiles. The current study thus provides new insights into differences in the active site topology of the investigated CYP2D isoforms.

Introduction

Human cytochrome P450 2D6 (CYP2D6) is one of the most important phase I enzymes involved in the metabolism of therapeutic drugs. Within the P450 superfamily, this enzyme is second to CYP3A4 in the number of drugs it biotransforms, holding a share of 20% versus 50% in the case of CYP3A4.[1] Another feature that has significantly contributed to the large interest CYP2D6 has obtained concerns its polymorphic nature.[2,3] To date, more than 70 different alleles have been identified.[4] The effects of these polymorphic genes range from a complete loss of functional protein to an increase in enzyme activity. Differences in substrate specificity may also arise. As a result, drug treatment in polymorphic individuals may cause adverse effects or a lack of drug efficacy.[5] To anticipate and prevent the occurrence of undesired effects resulting from drug therapies, an understanding of the ligand-binding specificity of CYP2D6 is needed. To acquire such understanding, knowledge of the active site topology and the effects of mutations on ligand binding is indispensable.

Initially, substrate and ligand-binding specificities concerning CYP2D isoforms were predominantly investigated by means of metabolism and binding studies in liver microsomes. The rat frequently served as an animal model for predicting drug toxicity and disposition in humans and is still frequently used for this purpose today. Regarded as a model for the "poor metabolizer" phenotype is the female Dark Agouti rat, which lacks the ability to metabolize selective CYP2D6 substrates such as debrisoquine and dextromethorphan.[6,7] With successful cloning and expression techniques, metabolism and inhibition studies have been performed with heterologously expressed CYP2D isozymes. The heterologous expression of CYP2D6 also prompted a range of other studies, which greatly facilitated the investigation of its active site topology and binding specificity. They include site-directed mutagenesis studies on key residues of CYP2D6 involved in ligand binding, e.g., Asp301,[8] and the development of high-throughput screening techniques for rapid identification of new ligands.[9,10] On the theoretical level, molecular modeling has been applied to study human CYP2D6. The combined efforts have led to a general perception of the CYP2D6 active site (reviewed by Ekins et al.[11]): the basic nitrogen atom of ligands generally interacts with a negatively charged residue located in the I helix (Asp301) or F helix (Glu216), and the aromatic moiety of ligands interacts with a phenylalanine (Phe481 or Phe483) located in the fifth β-sheet. In total, six structural elements or substrate recognition sites (SRSs) can be identified that contain ligand-binding residues.[12]

* To whom correspondence should be addressed. Phone: +31 20 4447590. Fax: +31 20 4447610. E-mail: vermeule@chem.vu.nl.
[†] Vrije Universiteit.
[‡] Osaka University Medical School.

10.1021/jm0209578 CCC: $25.00
Published on Web 12/05/2002

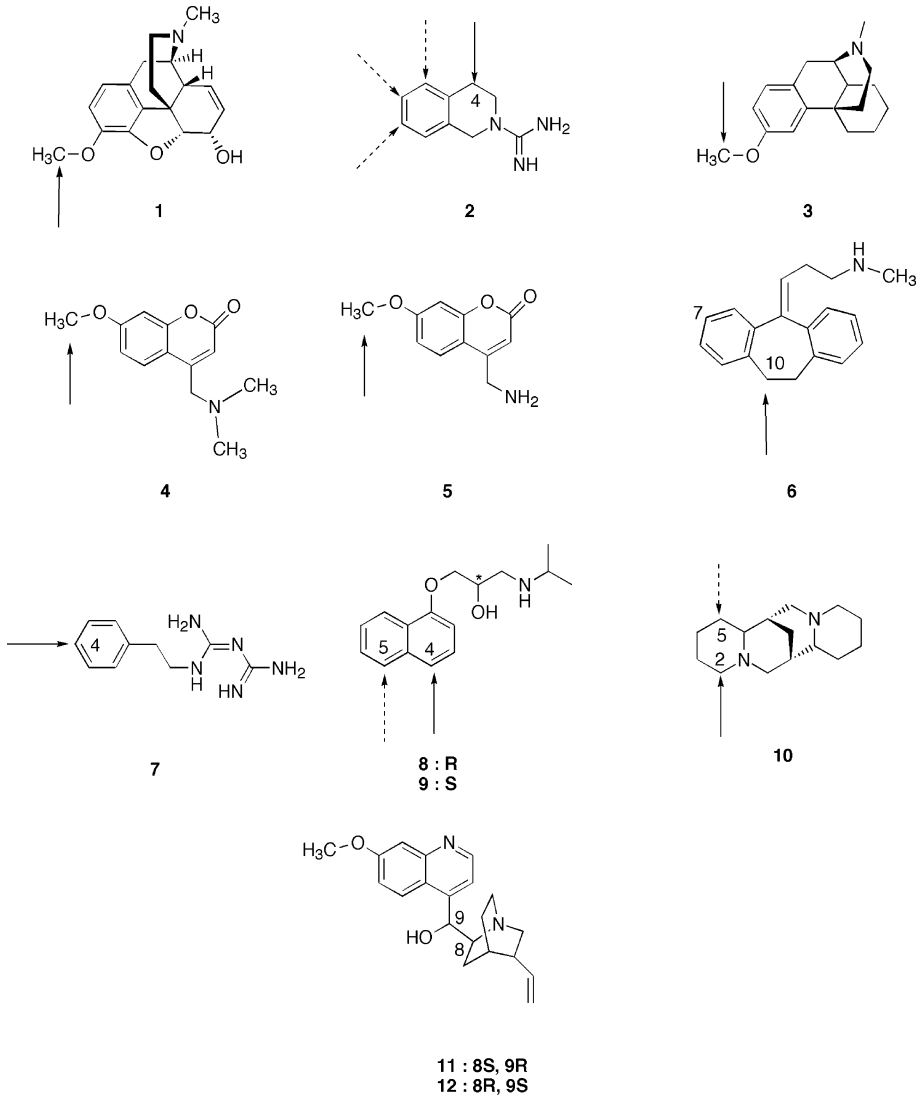

Figure 1. Chemical structure of the investigated ligands: (**1**) codeine; (**2**) debrisoquine; (**3**) dextromethorphan; (**4**) diMMAMC; (**5**) MAMC; (**6**) nortriptyline; (**7**) phenformine; (**8**) D- or *R*-propranolol; (**9**) L- or *S*-propranolol; (**10**) sparteine; (**11**) quinine; (**12**) quinidine. All compounds except the inhibitors **11** and **12** are substrates of CYP2D6. The corresponding site(s) of oxidation are indicated with (an) arrow(s). Dashed arrows indicate minor metabolic routes of CYP2D6. Numbers in the ring systems of **2** and **6**−**10** correspond to atom-numbering.

In contrast to humans, for which only one isoform (CYP2D6) has been identified, the rat contains six CYP2D isozymes: CYP2D1−5 and CYP2D18. Immunoblotting studies have demonstrated hepatic expression of CYP2D1, -2D2, -2D4, and -2D5, but not CYP2D3, in various rat strains.[6] CYP2D18 is believed to be the rat brain variant of CYP2D4.[13] The rat and human CYP2D isoforms share a high sequence identity (>70%). Nevertheless, significant differences in binding and (regioselectivity of) metabolism have been observed between these CYP2D isoforms.[6,7,14−16] For example, *R*-mianserin was N-oxidated by only CYP2D1 while 8-hydroxylation was performed by all investigated isoforms.[14]

Strongly homologous proteins can be perceived as a single isoform with a set of point mutations and may be used advantageously for increasing the knowledge and understanding of active site topologies. Here, the differences in binding specificities between rat CYP2D1−4 and human CYP2D6 were investigated. IC_{50} values of 11 structurally diverse compounds (Figure 1), known to competitively bind to CYP2D6, were determined for the five individual isoforms. The fluorescent probe 7-methoxy-4-(aminomethyl)coumarin[17] (MAMC (**5**)) was selected as a substrate, since it was expected that this compound was likely to have a similar affinity for the different isozymes because of its small size. The observed differences were rationalized by homology modeling and molecular dynamics (MD) studies on the CYP2D isoforms. A homology model of CYP2D6 was generated first using the recently crystallized rabbit CYP2C5 structure[18] as the template. The current study provides new knowledge on human and rat CYP2D active site topologies and elucidates which rat CYP2D isoforms are of dominating importance regarding ligand binding.

Materials and Methods

Chemicals. 7-Methoxy-4-(aminomethyl)coumarin (MAMC (**5**)), 7-hydroxy-4-(aminomethyl)coumarin (HAMC), and *N*,*N*-dimethyl-7-methoxy-4-(aminomethyl)coumarin (diMMAMC (**4**)) were synthesized as described previously.[17,19] Glucose 6-phosphate dehydrogenase and NADPH were from Boehringer (Mannheim, Germany) and Applichem (Darmstadt, Germany), respectively. Quinine (**11**) was purchased from Fluka (Zwijndrecht, The Netherlands), whereas D- and L-propranolol (**8**, **9**)

were from ICI (Macclesfield, U.K.). All other chemicals were obtained from Sigma Chemical Co. (St Louis, MO).

Microsomal Protein. Rat CYP2D isozymes were expressed in *Saccharomyces cerivisiae* as described previously,[16] resulting in P450 content of 2.5 nmol/mL CYP2D1, 0.25 nmol/mL CYP2D2, 0.36 nmol/mL CYP2D3, and 3.9 nmol/mL CYP2D4. The microsomes contained an optimized amount of coexpressed yeast cytochrome P450 reductase such that addition of rat NADPH cytochrome P450 reductase had no effect on catalytic activity.[16] Human CYP2D6 (2 nmol/mL; catalog no. P171), containing human NADPH cytochrome P450 reductase, was obtained from GENTEST Corp. (Woburn, MA). The reductase activity was 160 nmol/(min × mg of protein). None of the microsomes contained cytochrome b5 or a P450 other than the heterologously expressed CYP2D isoform. All P450 was in the form of holoprotein. Further details have been described by Wan et al.[16] and Penman et al.[20]

MAMC Metabolism by Rat CYP2D Isoforms. The metabolism of MAMC (**5**) by the different rat CYP2D isoforms and its time dependency were investigated by incubating 100 μM of MAMC at 37 °C in a 100 mM phosphate buffer, pH 7.4, containing microsomal protein and a NADPH-regenerating system (see below). Samples of 80 μL were drawn at intervals of 5 min for 30 min and added to 10 μL of 35% perchloric acid. After removal of the protein by centrifugation at 4000*g* for 20 min, metabolite identification and quantification were achieved by HPLC analysis as described below.

Enzyme Kinetics of MAMC O-Demethylation by Rat CYP2D Isoforms. The kinetic studies on rat CYP2D-mediated O-demethylation of MAMC (**5**) were performed in a 100 mM phosphate buffer, pH 7.4, using a final volume of 80 μL. Isozyme concentrations of 52.0, 3.1, 3.6, and 21.9 nM were used for respectively CYP2D1, -2D2, -2D3, and -2D4. Compound **5** was preincubated for 5 min at 37 °C in a final concentration range of 40−200 μM. The reaction was started by the addition of a preincubated NADPH-regeneration system, resulting in final concentrations of 1.3 mM NADPH, 3.3 mM glucose 6-phosphate, 3.3 mM $MgCl_2$, and 0.4 units/mL glucose 6-phosphate dehydrogenase. The reaction was stopped by the addition of 10 μL of 35% perchloric acid after 20 min (15 min in the case of CYP2D4). The samples were subsequently centrifuged at 4000*g* for 20 min, and 40 μL of supernatant was analyzed by means of HPLC as described below. Because of lower sensitivity, analysis could not be performed by means of a microplate reader.

Competition Studies. The competition studies with rat CYP2D isozymes were performed in the presence or absence of various concentrations of inhibitor, using MAMC (**5**) as a substrate. A final concentration of 100 μM was used for **5**, since this approximated its K_m value for all CYP2D isoforms. The incubations were furthermore carried out using the conditions described above.

In the case of CYP2D6, competition studies were performed using the microplate reader assay described previously.[19] Compound **5** was incubated in a final concentration of 10 μM, in the presence or absence of various concentrations of inhibitors. A CYP2D6 concentration of 1 nM was used.

HPLC Analyses. Chromatographic separation of **5** and its metabolite, HAMC, was achieved with an HPLC system consisting of model 300 and model 480 pumps (Gynkotek, Germering, Germany), two ChromSpher C18 columns (5 μm particles, 4.6 mm × 10 cm; Chrompack, Bergen op Zoom, The Netherlands), a Triathlon autosampler (Spark Holland, Emmen, The Netherlands), and a model 821-FP fluorescence detector (Separations B.V., The Netherlands). As eluent, a mixture of 15% methanol, 1% triethylamine, and 84% H_2O, adjusted to pH 3 using 70% perchloric acid, was used at a flow rate of 0.4 mL/min. To increase the fluorescent yield of the metabolite, the eluent was mixed postcolumn with a 0.1 M Tris-HCl solution, pH 9.0, at a flow rate of 0.4 mL/min. Detection was at an excitation wavelength of 370 nm (bandwidth 18 nm) and an emission wavelength of 470 nm (bandwidth 18 nm). A calibration curve of HAMC was used for quantification purposes.

Kinetics Analysis. K_m and V_{max} parameters, as well as IC_{50} values, were determined by using the nonlinear least-squares fitting method for one site binding and one site competition, respectively, as implemented in Prism 2.0.[21]

Model Building. The primary sequences of the rat and human CYP2D isozymes were obtained from the sequence retrieval system (SRS), accessible from the EMBL Internet site.[22] The Swiss protein accession numbers are P10633 (CYP2D1), P10634 (CYP2D2), P12938 (CYP2D3), P13108 (CYP2D4), and P10635 (CYP2D6). The crystal structure of rabbit CYP2C5[18] (PDB identifier 1DT6) was downloaded from the Brookhaven Protein Databank (PDB).[23] The CYP2D sequences were manually aligned with that of rabbit CYP2C5, using the homology module of InsightII,[24] which was implemented on a Silicon Graphics Octane R12000 (Silicon Graphics Inc.). Initially, a homology model was only made for CYP2D6 because this model could be validated on the basis of the large amount of experimental data available (see below). One-hundred models of the human isozyme were generated with the restraint-based comparative modeling program Modeller 4.0.[25] These models primarily differed in the conformation of part of the B/C loop and the F/G loop, since the former region possessed the largest insertions with respect to CYP2C5 and the latter region was lacking in the crystal structure. The four models with the best loop conformations and stereochemical parameters, as determined by visual inspection and PROCHECK,[26] were used for further validation and selection.

The final model of CYP2D6, resulting from the various validation steps (see below), was used as the template for modeling the rat CYP2D isoforms. The side chains of CYP2D6 were mutated to that of the corresponding rat enzyme using the homology module of InsightII,[24] after which a minimization was carried out with Amber 6.0[27] as described below.

Model Refinement and Validation. The first validation of the CYP2D6 models was achieved by establishing which of the four models was most able to accommodate the substrate codeine (**1**) in the orientation found by NMR spin-relaxation studies.[28] To this end, all four conformations of **1** were manually docked in the CYP2D6 active site using InsightII[24] in such a way that the methoxy group was directed toward the heme moiety while the basic nitrogen atom was directed toward either Asp301 or Glu216. The structures were minimized with 20 000 steps with Amber 6.0,[27] using the steepest descent method during the first 10 000 steps followed by the conjugate gradient minimizer. Simulated annealing was performed on the resulting structures by quickly heating the system to 600 K in 5 ps. The system was maintained at this temperature for 20 ps, after which it was gradually cooled to 0 K over 25 ps. During both the minimization and simulated annealing, a harmonic restraint (k = 1.0 kcal mol^{-1} Å^{-2}) was applied on the protein Cα trace, and a cutoff of 9 Å and a dielectric constant of 1 were used. During the simulated annealing, distance restraints were also applied on the unambiguously defined proton−Fe distances reported by Modi et al.,[28] using a force of 50 kcal mol^{-1} Å^{-2}.

Rigid Docking of Ligands. The CYP2D6 model found to be the most capable of satisfying the distance restraints for codeine (**1**), as deduced from spin-relaxation studies, was used for rigid docking studies on the 11 ligands investigated (Figure 1). This not only served the purpose of identifying interaction residues but was also used as a second validation step; binding orientations that are consistent with the known metabolic profiles of ligands should possess energetically favorable interaction energies. As a criterion for metabolism, a maximum distance of 5 Å between the site of oxidation, i.e., the carbon atom at which proton abstraction takes place, and the heme Fe atom (r(ox−Fe)) was used. The binding of quinine (**11**) and quinidine (**12**) could not be subjected to this validation, since these inhibitors are not metabolized by CYP2D6. Rigid docking studies with all CYP2D isoforms were performed with SACRD (simulated annealing with constrained rigid docking),[29] which uses a simulated annealing protocol and the cvff force field. The rigid protein model was defined by a 30 Å grid with grid points separated by 0.333 Å. The ligand was rigidly docked

into the active site pocket, which was defined by the center of the grid (chosen as Cβ of CYP2D6 residue 305), at high temperature. By gradual lowering of the temperature, the ligand adopted a low-energy binding orientation. To account for flexibility, different conformations of the ligand and protein structure were taken into account. In the case of the ligands, only conformers with energies less than 10 kcal/mol above that of the global minimum were docked. In the case of the protein, all sterically accessible rotamer combinations (rotamer library implemented in InsightII[24]) of residues 301, 216, and 483 were taken into account.

Dynamics. Molecular dynamics (MD) was performed on the CYP2D homology models for two purposes. The first is to examine whether the models were stable during dynamics. This was established by measuring the root mean square (rms) of the protein Cα trace of each MD frame compared to that of the starting structure. The second is to optimize the binding mode of a selected set of ligands resulting from the rigid docking procedure in order to rationalize the observed differences in IC_{50} values between CYP2D isoforms. All calculations were carried out with Amber 6.0,[27] using a dielectric constant of 1.0 and a cutoff of 9 Å. The system was solvated by a water shell of 9 Å, amounting to approximately 2000 water molecules, and neutralized with one to four sodium atoms using the Xleap routines implemented in Amber 6.0.[27] A minimization was subsequently performed as described above, after which 200 ps of unrestrained MD simulation followed. In the first 30 ps, the system was heated linearly from 10 to 300 K and was kept at this temperature for the remaining 170 ps.

Structure Generation and Charge Calculations of Ligands. Initial structures of the ligands studied were either obtained from the Cambridge Structural Database (CSD)[30] or generated with the Builder module of InsightII.[24] Subsequent minimization of the structures was performed with Discover implemented in InsightII,[24] using the cvff force field. Low-energy conformers of each structure were calculated by performing a Monte Carlo simulation using the cvff force field with the program CONF.[31] Atomic charges of the ligands were calculated in two different ways. For the rigid docking procedure with SACRD,[29] atomic charges were obtained by performing an AM1 single-point calculation with the Mopac/Ampac module implemented in InsightII.[24] Atomic charges to be used in the Amber 6.0[27] MD runs were essentially derived by electrostatic potential fitting as described by Cieplak et al.[32] for the AMBER force field. In short, electrostatic potentials were calculated for the four minimum energy geometries covering the broadest range of the conformational space of each ligand at the Connolly surface at 1.4, 1.6, 1.8, and 2.0 times the van der Waals radius using GAMESS US[33] and the SV 6-31G* basis set. The multiconformational restraint electrostatic potential (RESP) fitting procedure[34,35] was utilized to obtain atomic charges.

Electrostatic Potential Calculations. To rationalize the difference in overall binding affinity of the CYP2D isozymes for the studied ligands, the electrostatic potential of the enzymes were calculated with the DelPhi package[36,37] implemented in InsightII[24] using the continuum dielectric approach to solve the Poisson−Boltzmann equation by the finite difference method. Partial charges of the cvff force field for the enzymes at pH 7.4 were used. A constant ionic strength of 0.145 M was applied, as well as a dielectric constant of 4 for the protein and 80 for the solvent environment.

Results

Enzyme Kinetics of MAMC Metabolism by Rat CYP2D Isoforms. Investigation of MAMC (**5**) metabolism mediated by rat CYP2D isozymes, singly expressed in *Saccharomyces cerivisiae*, by HPLC showed that all four isoforms catalyzed only the O-dealkylation of the substrate to HAMC. Metabolite formation was found to be linear for 20 min in the cases of CYP2D1, -2D2, and -2D3. CYP2D4-mediated O-dealkylation of **5** was linear for 15 min only.

Table 1. Apparent Kinetic Parameters of MAMC (**5**) O-Dealkylation Mediated by Rat CYP2D1−4 Expressed in *Saccharomyces cerivisiae*, and Human CYP2D6 Expressed in a Human Lymphoblastoid Cell Line[a]

enzyme	K_m (μM)	V_{max} (min^{-1})	V_{max}/K_m (10^{-3} min^{-1}/μM)
CYP2D1	145 ± 41	0.048 ± 0.006	0.331 ± 0.135
CYP2D2	78 ± 6	0.895 ± 0.045	11.47 ± 1.45
CYP2D3	96 ± 12	0.760 ± 0.050	7.92 ± 1.50
CYP2D4	80 ± 10	1.122 ± 0.048	14.03 ± 2.36
CYP2D6[b]	11.5 ± 1.3	2.81 ± 0.14	244 ± 39

[a] Measurements are shown as the mean ± SD ($n = 3$). [b] Determined previously by Venhorst et al.[19]

The O-dealkylation of **5** exhibited Michaelis−Menten kinetics for all four rat CYP2D isozymes. The isoforms were found to have comparable K_m values ranging between 78 and 145 μM (Table 1). The V_{max} values of the CYP2D isozymes for this reaction were also the same order of magnitude with the exception of CYP2D1 (Table 1). The latter displayed a notably lower maximal rate of O-dealkylation of **5** with a V_{max} value of 0.048 ± 0.006 min^{-1} and correspondingly had the lowest intrinsic clearance (V_{max}/K_m). CYP2D6 has previously been shown to O-dealkylate **5** with low K_m and high V_{max} values of 11.5 ± 1.3 μM and 2.81 ± 0.14 min^{-1}, respectively.[19]

Competition Studies. Table 2 lists the IC_{50} values of 11 investigated CYP2D6 model substrates and inhibitors toward the rat and human CYP2D isoforms. When the CYP2D2 and -2D6 inhibition data are examined, it is striking that their IC_{50} values are generally much lower than those of CYP2D1, -2D3, and -2D4. When the rat CYP2D inhibition data were correlated linearly with that of human CYP2D6 (excluding quinidine (**12**)), a significant correlation ($R^2 = 0.739$; leave-one-out validation, $0.692 < R^2 < 0.805$) between the IC_{50} values of the compounds investigated was only obtained for CYP2D2. A significant correlation furthermore existed between rat isoforms CYP2D3 and -2D4 ($R^2 = 0.756$; leave-one-out validation, $0.664 < R^2 < 0.834$). All other R^2 values were smaller than 0.454. Interestingly, sparteine (**10**) and phenformine (**7**) did not inhibit CYP2D1-mediated O-demethylation of **5**. Instead, a potentiation was observed. At an inhibitor concentration of 1 mM, HAMC formation was increased 3-fold and 5-fold in the presence of **10** and **7**, respectively.

A very notable difference between human CYP2D6 and the rat CYP2D isoforms was observed when comparing their respective affinities for the inhibitors quinine (**11**) and quinidine (**12**). Of these compounds, CYP2D1 and CYP2D6 displayed the lowest IC_{50} value toward **12**. The difference in IC_{50} value between **11** and **12** was only about 2-fold in the case of CYP2D1, but **12** had a 184-fold lower IC_{50} value than **11** in the case of CYP2D6. The other CYP2D isozymes were inhibited to the largest extent by **11**. The isomers D- and L-propranolol (**8**, **9**) displayed similar IC_{50} values toward all CYP2D isoforms investigated with the exception of rat CYP2D1 where the D-isomer displayed a 3-fold higher affinity. Sparteine (**10**) and codeine (**1**) generally exerted a low inhibitory potency on the CYP2D isoforms. Compound **1** was the weakest inhibitor in the case of all isoforms except CYP2D2. For the latter, however, only diMMAMC (**4**) showed an even lower inhibitory potency. CYP2D2 furthermore displayed a relatively low

Table 2. IC_{50} Values of Compounds for MAMC (**5**) O-Dealkylation Mediated by Rat and Human CYP2D Isozymes ($n \geq 2$, Measured on Separate Days)[a]

ligand	IC_{50} (μM) CYP2D1	IC_{50} (μM) CYP2D2	IC_{50} (μM) CYP2D3	IC_{50} (μM) CYP2D4	IC_{50} (μM) CYP2D6
1 codeine	1320 ± 192	238 ± 34	4089 ± 560	2216 ± 119	104 ± 27
2 debrisoquine	529 ± 96	107 ± 3	1754 ± 105	747 ± 50	23.8 ± 3.2
3 dextromethorphan	264 ± 17	5.6 ± 0.1	18.6 ± 0.5	136 ± 31	1.8 ± 0.4
4 diMMAMC	329 ± 112	307 ± 3	862 ± 34	1178 ± 543	74.2 ± 15.6
6 nortriptyline	204 ± 15	1.9 ± 0.3	14.2 ± 0.1	19.3 ± 0.1	2.3 ± 0.2
7 phenformine		45.4 ± 8.5	1927 ± 204	833 ± 86	27.0 ± 5.0
8 D-propranolol	182 ± 25	0.42 ± 0.22	155 ± 16	117 ± 38	1.9 ± 0.7
9 L-propranolol	571 ± 16	0.35 ± 0.25	172 ± 3	133 ± 15	1.4 ± 0.5
10 sparteine		7.2 ± 2.7	2146 ± 307	1487 ± 23	66.4 ± 17.6
11 quinine	46.5 ± 7.6	0.094 ± 0.009	12.0 ± 0.2	1.7 ± 0.4	0.61 ± 0.05
12 quinidine	19.9 ± 1.9	2.8 ± 0.7	26.9 ± 4.4	47.2 ± 13.4	0.0033 ± 0.0010

[a] Rat CYP2D1 to CYP2D4 was expressed in *Saccharomyces cerivisiae*, and human CYP2D6 was expressed in a human lymphoblastoid cell line. IC_{50} values of phenformine (**7**) and sparteine (**10**) could not be determined for CYP2D1 because these compounds had a stimulatory effect on HAMC formation.

IC_{50} value for **10** when compared to the other isozymes. The CYP2D6 model substrates debrisoquine (**2**) and dextromethorphan (**3**) generally possessed an intermediate to low inhibitory potency.

The CYP2D6 Homology Model. Figure 2 displays the sequence alignment of CYP2D6 (and the investigated rat CYP2D isoforms) with rabbit CYP2C5,[18] which was used as the template for constructing the homology model. The final model possessed good stereochemical quality, as determined by PROCHECK,[26] with the backbone Φ and Ψ dihedral angles of 98% of the residues located within the generously allowed regions (68% core) of the Ramachandran plot. The CYP2C5 template structure also had 98% of its residues located in the generously allowed regions, with 71% of the residues in the core of the Ramachandran plot. The final model was well able to accommodate codeine (**1**) in the conformation determined by NMR spin-relaxation studies,[28] as shown in Table 3. Moreover, this orientation corresponded to an energetically favorable binding mode, since **1** formed a hydrogen bond with Glu216 (Figure 3). Other prominent interaction residues included Phe120, providing π-stacking interaction, and Phe483, providing van der Waals interaction (Figure 3).

Automated and therefore unbiased rigid docking studies with SACRD[29] revealed that the CYP2D6 homology model was able to accommodate all 10 substrates in the binding mode(s) corresponding with their reported metabolic route(s) (Table 4 and Figure 1). The known sites of oxidation were directed toward the heme iron and are located within 5 Å of this atom. The fact that these binding modes, with the exception of nortriptyline (**6**), included the docking orientation with the highest interaction energy further supported the validity of the model. In the case of **6**, the docking orientation listed in Table 4 had the second highest interaction energy. The energetically most favored binding mode corresponded to aromatic 7-hydroxylation (Figure 1).

As shown in Table 4, all CYP2D6 substrates except sparteine (**10**) had an interaction with either Glu216 or Asp301. Some substrates, e.g., propranolol (**8**, **9**), appeared to hydrogen-bond exclusively to one of these negatively charged residues. Debrisoquine (**2**), dextromethorphan (**3**), MAMC (**5**), and phenformine (**7**), however, appeared to use both Glu216 and Asp301 as alternative anchors for their basic nitrogen atoms. In the case of **2**, the rigid docking study suggested that the different phenolic products, constituting 64% of total

Table 3. Ability of the CYP2D6 Homology Model To Accommodate Codeine (**1**) in the Binding Mode Determined by Experimental Spin-Relaxation Studies[a]

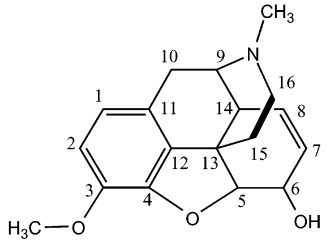

atom	r(H−Fe) CYP2D6 model (Å)	r(H−Fe) experimental (Å)
C1H	7.6	7.5 ± 0.2
C2H	5.1	5.0 ± 0.1
C5H	8.9	9.1 ± 0.1
C6H	10.0	10.0 ± 0.2
C7H	9.7	9.3 ± 0.3
C8H	10.6	10.2 ± 0.2
C9H	11.4	11.2 ± 0.2
C15Ha[b]	9.2	9.3 ± 0.1
C15Hb[b]	10.6	10.8 ± 0.2
∼N−CH3[b]	12.3	12.1 ± 0.2
∼O−CH3[b]	3.6	3.1 ± 0.1

[a] Reference 28. The distances between the protons of **1** and the iron atom of the CYP2D6 heme group obtained after simulated annealing of the ligand−enzyme complex with distance restraints are listed, as well as those reported by Modi et al.[a] Numbering of the protons is according to the C atom numbers. [b] Not included in the distance restraints.

metabolite formation,[38] arise from virtually the same binding mode. In this light, the designation of 4-hydroxylation as the major metabolic route appears misguided. A feature common to all observed binding modes was the involvement of Phe120, equivalent to Ala113 in CYP2C5, in π-stacking with aromatic moieties of the ligands. Residues Ile106, Leu213, Ala305, Val308, Val370, Val374, and Phe483 were generally involved in hydrophobic interactions (see also Table 5). Another interesting observation resulting from the rigid docking experiments was that a single rotamer of Asp301 was observed in the favored binding orientations. In this conformation, the carboxylate group of Asp301 hydrogen-bonds with the backbone nitrogen atoms of Val119 and Phe120, thus stabilizing the B/C loop.

In additional studies on the binding mode of a selected set of ligands, MD simulation was carried out to further optimize the ligand−enzyme interactions. On the basis of Table 4, all CYP2D−ligand complexes possessing a ligand binding energy within 15 kcal/mol of the highest

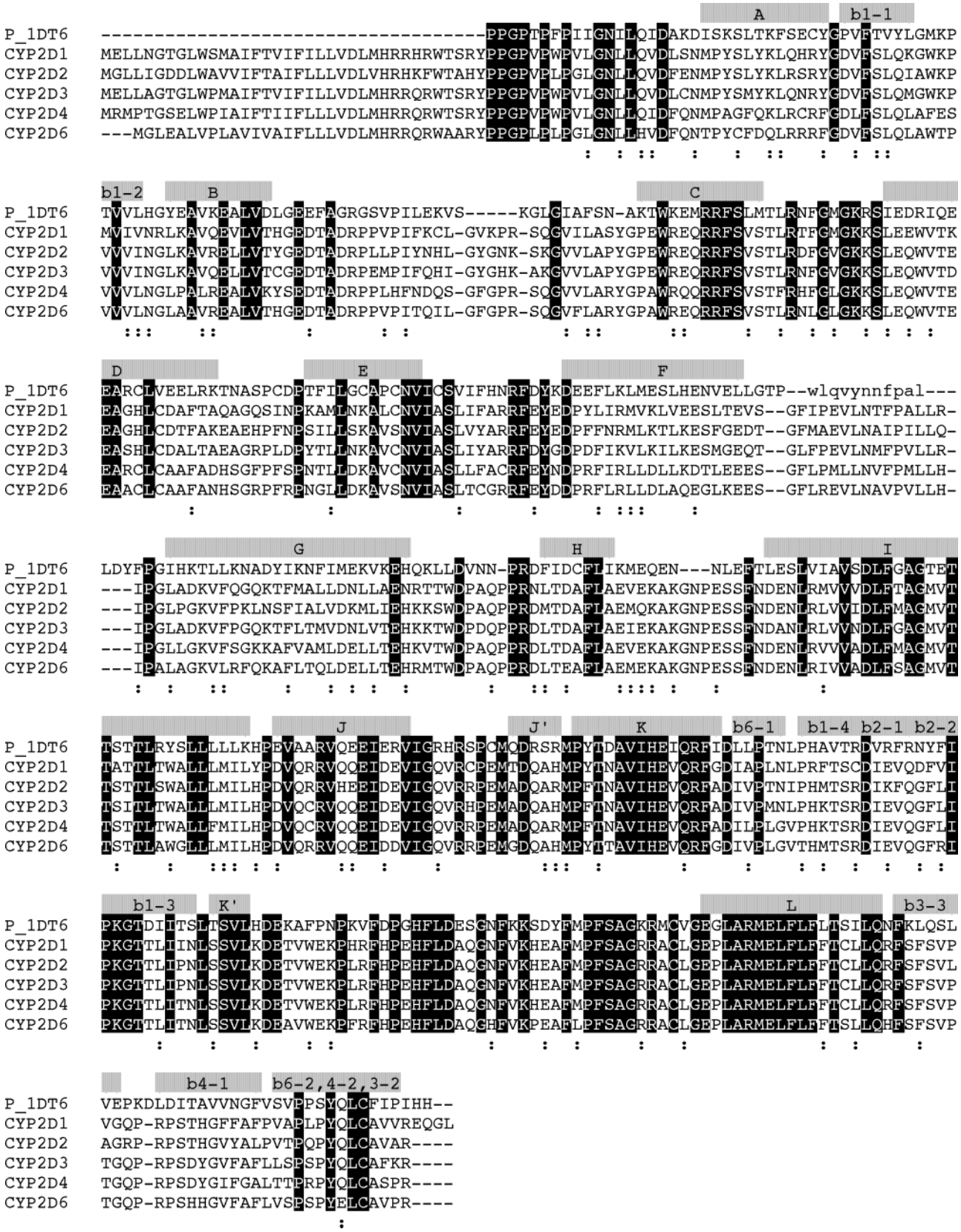

Figure 2. Alignment of the sequences of the investigated rat and human CYP2D isozymes with that of the crystallized rabbit CYP2C5 PDB structure 1DT6 used as input for the comparative modeling program Modeller. Gray bars indicate secondary structure elements. α-Helices and *β*-sheets respectively indicated by a capital and the character "b" are named and numbered in analogy to Hasemann et al.[56] Invariant residues are shown in black boxes, whereas conserved substitutions are indicated by a colon. Residues that were mutated in the crystallized CYP2C5 structure[55] are underlined, and small characters indicate residues that were missing from the 3D structure.

interaction energy observed for that ligand were further investigated.

CYP2D Active Site Topologies. MD studies on the binding of MAMC (**5**) in the CYP2D6 model demon-

Table 4. Results of Rigid Docking of the Investigated CYP2D6 Substrates in the Active Site of the CYP2D6 Homology Model[a]

substrate	oxidation site	*r*(ox−Fe) (Å)	∂*E* (kcal/mol)	residue
1 codeine	∼OCH_3	5.0	0	Glu216
2 debrisoquine	aromatic[b]	4.5	0	Glu216 + Asp301
	4-position	3.9	13	Asp301
3 dextromethorphan	∼OCH_3	4.7	0	Asp301[c]
4 diMMAMC	∼OCH_3	4.1	0	Asp301
5 MAMC	∼OCH_3	3.7	0	Glu216[d]
6 nortriptyline	E-10-position	4.1	9	Glu216
7 phenformine	4-position	4.0	0	Glu216 + Asp301
8 D-propranolol	5-position	4.1	0	Glu216
	4-position	5.0	2	Glu216
9 L-propranolol	5-position	4.5	0	Glu216
	4-position	5.0	4	Glu216
10 sparteine	5-position	4.8	0	
	2-position	5.0	1	

[a] Listed are the site of oxidation (Figure 1), the distance between the oxidation site of the substrate and the heme iron atom (*r*(ox−Fe)), the difference in interaction energy (∂*E*) between the listed orientation and the one displaying the highest interaction energy as calculated with the cvff force field, and the residue interacting with the basic nitrogen moiety of the substrate. See text and Table 5 for other ligand-binding residues. [b] The binding modes corresponding to aromatic hydroxylation at different positions varied only slightly in orientation and subsequently had comparable binding energies. [c] A hydrogen bond with Glu216 was also observed for another orientation with ∂*E* < 15 kcal/mol. [d] A hydrogen bond with Asp301 was also observed for another orientation with ∂*E* < 15 kcal/mol.

Table 5. Active Site Residues of Human and Rat CYP2D Isoforms and Rabbit CYP2C5 Whose Side Chains Are Involved in Ligand Binding[a]

SRS	residue number[b]	residue CYP2D1	residue CYP2D2	residue CYP2D3	residue CYP2D4/18	residue CYP2D5	residue CYP2D6	residue CYP2C5
1	103	Pro	Leu	Glu	Pro	Pro	Pro	Ser
	105	Pro	Pro	Pro	His	Pro	Pro	Pro
	106	Ile	Ile	Ile	Phe	Ile	Ile	Ile
	112	Val	Tyr	Tyr	Phe	Val	Phe	Ser
	120	Ile	Val	Val	Val	Val	Phe	Ala
	121	Leu	Leu	Leu	Leu	Phe	Leu	Phe
2	213	Leu	Phe	Met	Leu	Leu	Leu	Val
	216	Val	Asp	Gln	Glu	Val	Glu	Leu
	217	Ser	Thr	Thr	Ser	Ser	Ser	Ser[c]
3	243	Gly	Lys	Gly	Gly	Gly	Phe	Asn
	244	Gln	Leu	Gln	Lys	Gln	Gln	Ala
4	**301**	**Asp**	**Asp**	**Asp**	**Asp**	**Asp**	**Asp**	**Asp**
	304	Thr	Met	Gly	Met	Thr	Ser	Gly
	305	**Ala**	**Ala**	**Ala**	**Ala**	**Ala**	**Ala**	**Ala**
	308	Val	Val	Val	Val	Val	Val	Glu
	309	**Thr**	**Thr**	**Thr**	**Thr**	**Thr**	**Thr**	**Thr**
5	369	Ile	Ile	Ile	Ile	Ile	Ile	Leu
	370	Ala	Val	Val	Leu	Ala	Val	Leu
	374	Leu	Ile	Leu	Val	Leu	Val	Leu
	375	Pro	Pro	Pro	Pro	Pro	Thr	Thr
6	483	Phe	Leu	Phe	Ala	Ile	Phe	Phe
	484	Pro	Pro	Leu	Leu	Ser	Leu	Val

[a] The interaction residues were determined by rigid docking studies on 12 substrates and inhibitors (Figure 1) in the binding pocket of CYP2D6. Residues shown in bold are invariant in all investigated enzymes. [b] Residue numbering is that of CYP2D6. [c] Mutated to Gly in the crystallized CYP2C5 structure.[55]

strated that the homology model was stable (Figure 4) and that **5** maintained an orientation enabling O-demethylation (average *r*(ox−Fe) = 4.5 Å over the last 100 ps). The CYP2D6 homology model thus performed satisfactorily on all validation steps applied and was therefore used as the template to construct models of CYP2D1, -2D2, -2D3, and -2D4. Rigid docking studies of **5** followed by 200 ps of MD simulation showed that these models were also stable and corresponded to the experimentally observed O-dealkylation of **5**. Final rms values and average *r*(ox−Fe) distances were all below 1.8 and 4.7 Å, respectively. The amino acid residue favored in binding the basic nitrogen of **5** was Asp301 (throughout the manuscript, residue numbering is according to the homologous residue in CYP2D6) for all rat isoforms except CYP2D2. In the case of CYP2D2, Asp216 (Table 5) acted as charge partner.

Table 5 lists the active site residues of human CYP2D6 and rat CYP2D1−4, as deduced from the rigid docking studies. The analogous residues in CYP2D5 and -2D18 have also been included. CYP2D4 and -2D18 were found to differ in the identity of only four residues, none of which were located in the CYP2D active site. When the active site residues of the human and rat CYP2D isoforms listed in Table 5 are examined, it is striking how few residues in the models are completely conserved. Only five of the 22 residues are invariant in all human and rat CYP2D isozymes, of which four are located in the I helix (SRS 4). Correspondingly, sequence identities between CYP2D isoforms were much lower for the active site residues than for the overall sequences (Table 6) except between CYP2D4 and -2D18. The most notable differences in active site residues of the homology models between human and rat isoforms involved

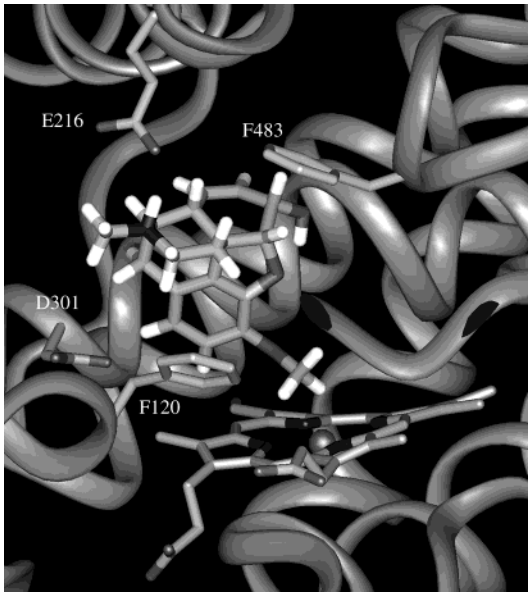

Figure 3. Obtained binding orientation of codeine (**1**) in the active site of CYP2D6 after simulated annealing with distance restraints applied on the distance between the uniquely defined protons of **1** and the Fe atom of the porphyrine ring of the enzyme, as observed by Modi et al. (see Table 3).[28] In the observed binding mode, **1** forms a hydrogen bond with Glu216. Asp301 was not involved in binding the basic nitrogen atom of **1** but instead hydrogen-bonded with the backbone nitrogen atoms of residues 119 and 120. The two phenylalanine residues located in the CYP2D6 active site provided either $\pi-\pi$ stacking (Phe120) or van der Waals (Phe483) interactions.

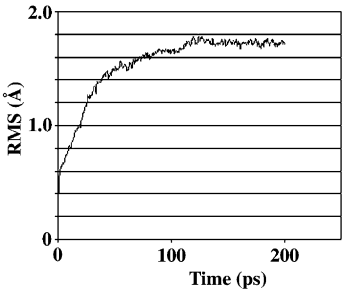

Figure 4. The rms values (Å) of the protein Cα trace of the CYP2D6−MAMC complex compared to the starting structure, plotted for each frame (0.5 ps) of the MD run.

residues 120 and 216. As described above, residue 120 constitutes a phenylalanine in CYP2D6 and provides π-stacking interactions with ligands. In all rat isoforms, residue 120 is nonaromatic and therefore only capable of contributing to ligand binding affinities by van der Waals interactions. The rigid docking studies with CYP2D6 identified Glu216 as a key ligand-binding residue forming hydrogen bonds with several substrates. In the cases of CYP2D1/5 and -2D3, a valine and glutamine, respectively, are located at this position. These are unable to form a salt bridge with the basic nitrogen of ligands. The glutamine residue in CYP2D3 is capable of forming a weaker hydrogen bond interaction.

Calculation of electrostatic potentials of the CYP2D active sites demonstrated large differences as shown in Figure 5. CYP2D6 and -2D2 displayed a distinctly negative electrostatic potential in and around their binding pocket. The active site of CYP2D1, however, was found to be largely neutral in electrostatic potential. CYP2D3 and -2D4 displayed large areas of both neutral and negative electrostatic potential.

Table 6. Sequence Identities (%) of Rat and Human CYP2D Isoforms and Rabbit CYP2C5[a]

	CYP2D1	CYP2D2	CYP2D3	CYP2D4	CYP2D5	CYP2D18	CYP2D6	CYP2C5
CYP2D1		73	79	72	95	72	71	39
CYP2D2	45		78	73	73	73	71	41
CYP2D3	59	59		75	79	75	72	41
CYP2D4	50	41	45		73	99	77	39
CYP2D5	82	41	55	50		73	71	39
CYP2D18	50	41	45	100	50		77	39
CYP2D6	59	41	55	59	50	59		40
CYP2C5	41	27	41	27	41	27	32	

[a] Both the overall sequence identity (upper triangle) and that of the active site residues listed in Table 5 (lower triangle) are given.

MD Simulations of the Binding Mode of Quinidine, Quinine, and Sparteine in Rat CYP2D2 and Human CYP2D6. Marked differences were observed in the IC_{50} values of quinidine (**12**), quinine (**11**), and sparteine (**10**) toward CYP2D2 and CYP2D6. The corresponding binding modes of these compounds after rigid docking were therefore further investigated by MD simulations. All complexes were stable and had a final rms value below 1.9 Å. Parts A and B of Figure 6 display the observed favored binding mode of **12** in CYP2D2 and -2D6. In the orientation observed for CYP2D6, the basic nitrogen of **12** formed a hydrogen bond with Asp301, and its hydroxyl group hydrogen-bonded with the backbone carbonyl of Ser304. Simultaneously, the quinoline nitrogen was located directly above the heme iron atom (average N−Fe distance over the last 100 ps of 4.1 Å), donating its lone pair. π-Stacking interaction was observed with Phe120 of CYP2D6. Because of the more bulky residues surrounding Asp301 in CYP2D2 (Val120 and Met304; Table 5), the quinoline nitrogen of **12** was unable to approach the heme iron atom closely while maintaining a strong interaction with Asp301. As a result, the average distance between the quinoline nitrogen and Fe over the last 100 ps was 5.1 Å, whereas the nitrogen lone pair did not point toward the Fe atom. Compound **12**, however, was able to form a hydrogen bond with the backbone carbonyl of Met304, analogous to that observed for Ser304 of CYP2D6.

As for **12**, modeling studies suggested the involvement of Asp301 in binding the basic nitrogen of quinine (**11**) in CYP2D6 (Figure 6D). Because of the inverted chiral centers, however, **11** adjusted its binding mode such that the hydroxyl group of this stereoisomer displayed a hydrogen bond with the backbone carbonyl group of Asp301. The quinoline nitrogen was unable to donate its lone pair to the heme iron atom. This observation was also made for the binding mode of **11** in CYP2D2 (Figure 6C), although the average N−Fe distance during the last 100 ps of MD was somewhat smaller (5.1 vs

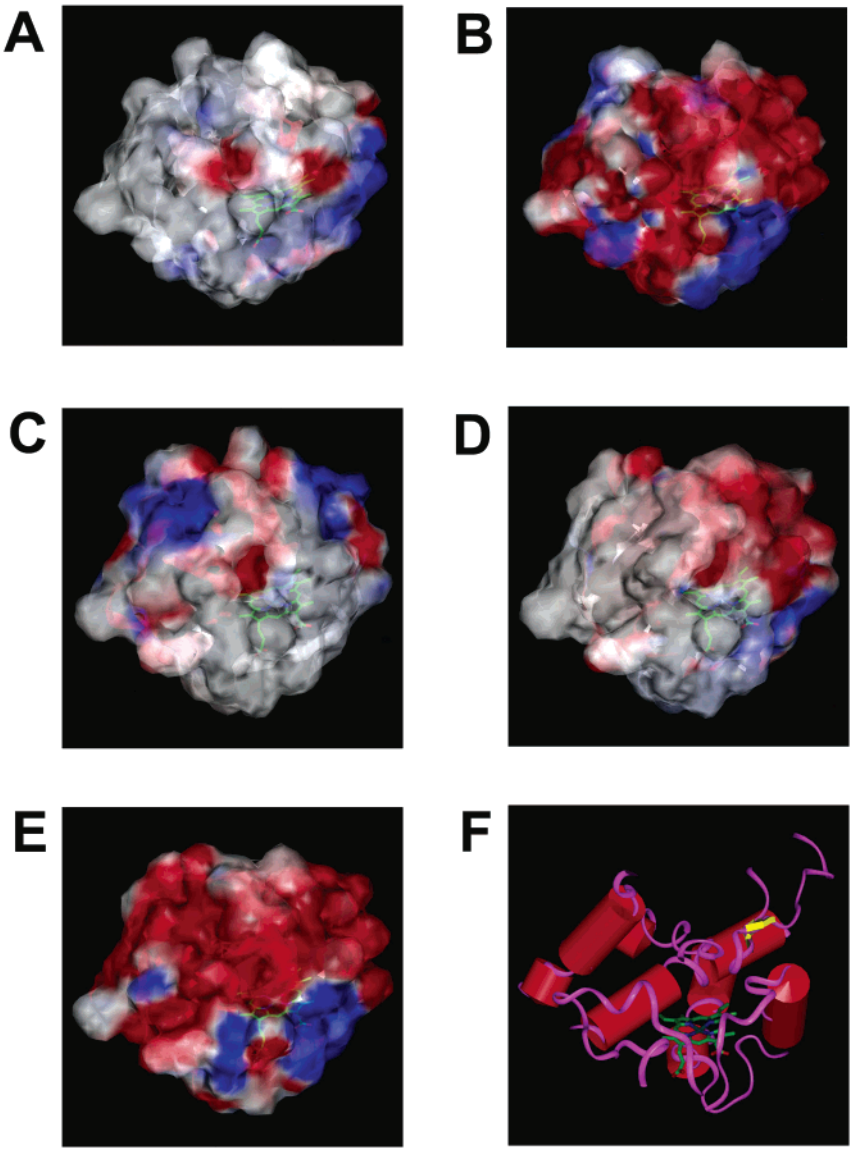

Figure 5. Electrostatic potentials of the active sites of (A) CYP2D1, (B) CYP2D2, (C) CYP2D3, (D) CYP2D4, and (E) CYP2D6. Red, blue, and white respectively indicate negative, positive, and neutral electrostatic potentials. The electrostatic potential surfaces correspond to the orientation of the active site shown in (F), with the heme group forming the bottom of the active site.

5.6 Å) and the quinoline nitrogen lone pair was directed toward the heme iron atom. In contrast to CYP2D6, Asp216 was involved in anchoring the basic nitrogen of **11** in the CYP2D2 model. Additionally, Thr217 hydrogen-bonded with the protonated moiety of **11**. The hydroxyl group of **11** displayed a hydrogen bond with the backbone carbonyl of Met304 of CYP2D2.

In the preferred binding mode of sparteine (**10**) in CYP2D2 and -2D6 (parts E and F of Figure 6), a hydrogen bond with an active site residue was not observed. Compound **10** can adopt two conformations under physiological conditions[39] in which the compound has also been crystallized.[30] One of these contains an internal hydrogen bond, and it was this conformation that was found to be most favorable in binding to the active site of both CYP2D2 and -2D6. As shown in parts E and F of Figure 6, the binding orientation differed significantly in the two isozymes, although both orientations corresponded to metabolism at the C2 position (Figure 1), as also observed experimentally.[39,40] The average *r*(ox−Fe) was 4.8 Å for CYP2D6 and 4.9 Å for CYP2D2.

Discussion

In this study the ligand-binding specificities and active site topologies of rat and human CYP2D isoforms, i.e., rat CYP2D1−4 and human CYP2D6, were investigated. To this end, the enzyme kinetics of O-demethylation of the substrate MAMC (**5**) was investigated for all CYP2D isoforms. Subsequently, IC_{50} values of 11 structurally diverse ligands were determined experimentally (Table 1) and homology models of all five proteins were generated for rationalization purposes. Until now, homology modeling of CYP2D members has been limited to CYP2D6.[11]

Correlation studies for the experimentally determined IC_{50} values showed that rat CYP2D2 resembled the human isoform CYP2D6 the most in terms of ligand-binding specificity. This is surprising because CYP2D2 displayed the lowest identity with CYP2D6 in both the

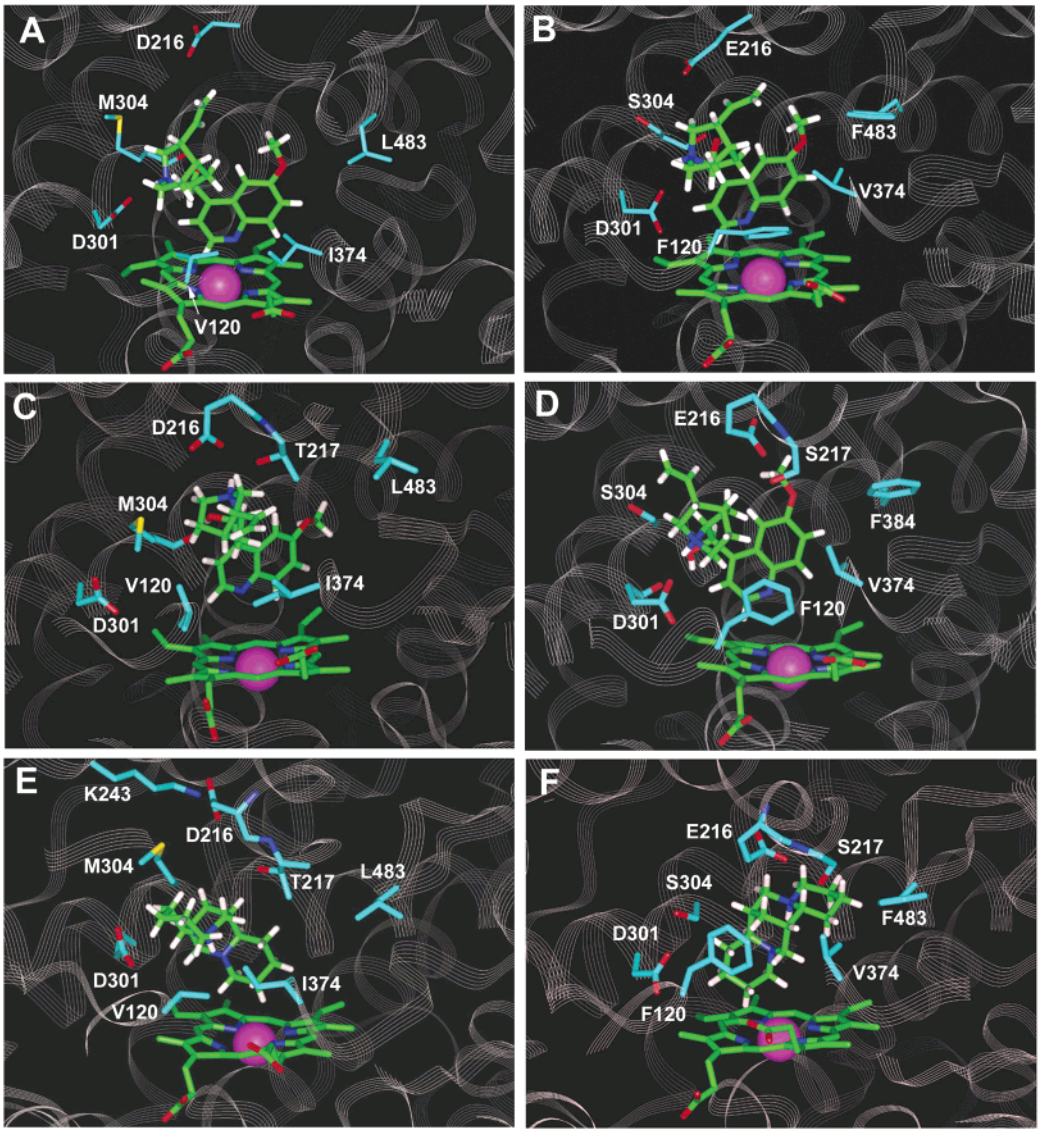

Figure 6. Observed binding mode resulting from MD simulation of (A) quinidine (**12**) in CYP2D2, (B) **12** in CYP2D6, (C) quinine (**11**) in CYP2D2, (D) **11** in CYP2D6, (E) sparteine (**10**) in CYP2D2, (F) **10** in CYP2D6. The heme iron atom is shown in CPK and is magenta. The heme group, ligand, and side chains (blue) are shown in stick form. The residue numbers of the various side chains are listed as well.

overall sequence (71%; Table 6) and active site residues (41%; Table 6). The generally lower IC_{50} values observed for CYP2D2 compared to the other three rat CYP2D isozymes investigated indicate a dominating role for this isoform in ligand binding. This is supported by the 30- to 40-fold lower hepatic expression level of CYP2D2 in the female Dark Agouti rat, a model for the CYP2D6 poor metabolizer phenotype, compared to Sprague−Dawley or Wistar rats. CYP2D1 and -2D4 hepatic expression levels were higher in the female Dark Agouti than in Sprague−Dawley or Wistar rats, suggesting that these enzymes are not essential for CYP2D activity in the rat.[6,7] The hepatic expression of CYP2D5 in Dark Agouti rats, its absence in Wistar rats, and the high sequence identity with CYP2D1 all appear to also exclude CYP2D5 as an important drug-metabolizing rat CYP2D isoform. Interestingly, the current competition studies revealed an increase in CYP2D1-mediated metabolism of **5** in the presence of both phenformine (**7**) and sparteine (**10**). This potentiation is likely indicative of cooperative binding, which so far has only been reported for human CYP3A4.[41,42]

The current CYP2D6 model was based on the crystallized CYP2C5 structure, which is the first mammalian CYP with resolved 3D structure.[18] Given the higher sequence identity of CYP2D isoforms with CYP2C5 (39−41%) compared with bacterial P450s (15−20%), the current homology model should present a significant improvement over previous ones. This is supported by the fact that this is the first CYP2D6 model that has been successfully subjected to MD simulation and demonstrated to be stable (Figure 4). The previously modeled CYP2D6 structures were either based on a single bacterial P450 (P450 cam;[43] P450 BM3[44]) or based on several P450 structures (P450s BM3, CAM, and terp[28,45−47]). The use of different templates not only results in differences in the relative position of active site residues. In combination with shifts in the alignment, the identity of active site residues may also differ. Phe120 and Glu216, reported here as key interaction residues, are not located in the active site of several previously reported CYP2D6 models.[28,47] Moreover, Phe481, and not Phe483, has been identified as the SRS 6 key interaction residue in the model by de Groot et

al.[46] The use of different templates may explain the difference in binding orientation of codeine (**1**) in the current CYP2D6 model and that by Modi et al.[28] In the current model, Glu216 interacts with the basic nitrogen of **1**, whereas in the latter model Asp301 fulfills this role.

The current identification of Glu216,[48] Asp301,[8,49] Val374,[50] and Phe483[51] as active site residues is experimentally supported by respective mutation studies on CYP2D6. Metabolism studies on four substrates with a CYP2D6 Ser304Ala mutant showed that this residue did not play a key role in substrate binding because this mutation had only a small effect on K_m values of the investigated substrates and did not influence the IC_{50} values of quinine (**11**) and quinidine (**12**) toward CYP2D6.[52] On the basis of the current CYP2D6 homology model, it is not surprising that the Ser304Ala mutation had little effect, since only Cβ of Ser304 displayed contact with ligands. Its hydroxyl group hydrogen-bonded with the carbonyl oxygen of Ala300. On the basis of the present rat CYP2D2 homology model, an effect on substrate binding would be expected by a Ser304Met mutation because the side chain of this residue was directed toward the CYP2D2 active site.

The current modeling studies suggested that Asp301 has a 2-fold function. Apart from interacting with the basic nitrogen atoms of ligands (Table 4), it additionally appeared to stabilize the B/C loop by hydrogen-bonding to the backbone nitrogens of residues 119 and 120. This interaction was also observed for the analogous residues in the CYP2C5 crystal structure.[18] The importance of Asp301 in stabilizing protein structures is further supported by the observation that human CYP2C enzymes also contain this residue,[53] whereas CYP2C enzymes are not recognized to favor the binding of basic ligands. The recent mutation studies on Asp301 in CYP2D6 by Hanna et al. also indicated a structural role for this residue.[49]

When human CYP2D6 is compared with the rat CYP2D isoforms, one of the most striking features is the variation in the residue at position 216, which was found to be a valine (CYP2D1/5), aspartate (CYP2D2), glutamine (CYP2D3), or glutamate (CYP2D4/6/18) (Table 5). The absence of any hydrogen-bonding capacity in this F helix residue in CYP2D1 may explain why a correlation between CYP2D1 and CYP2D6 was not even observed in the trend of IC_{50} values. Intuitively, it is tempting to correlate the lack of a strong hydrogen bond acceptor in the F helix with the higher IC_{50} values observed for CYP2D1 and CYP2D3 compared to CYP2D2. This, however, does not explain the overall high IC_{50} values observed for CYP2D4, which possesses a glutamate at position 216. The differences in absolute IC_{50} values could be further rationalized by the electrostatic potential of the respective CYP2D active sites. Whereas both CYP2D2 and -2D6 displayed an active site surface with a clear negative electrostatic potential overall, CYP2D1, -2D3, and -2D4 showed large surface areas that were neutral (Figure 5). It thus appears that the electrostatic potential of the active site significantly affects the overall binding affinity of ligands, as also described by Wade et al.,[54] by influencing the tightness of ligand binding in the active site and/or by long-range attraction.

MD studies showed that in both the active site of CYP2D2 and -2D6 quinidine (**12**) was able to form a strong hydrogen bond between its basic nitrogen and Asp301 while its hydroxyl group interacted with the carbonyl group of residue 304 (parts A and B of Figure 6). Unique to the binding mode in CYP2D6, however, was the interaction of the quinoline nitrogen with the heme iron atom. This heme ligation may explain the large difference (>800-fold) in IC_{50} value for **12** between CYP2D2 and -2D6 (Table 2). The difference in IC_{50} value between these two isozymes for quinine (**11**) was less extreme than observed for **12**. Correspondingly, the higher inhibitory potency of **11** in CYP2D2 (~6-fold) may be rationalized by the observed additional hydrogen bond between its basic nitrogen and Thr217. Although the most favored binding mode, as deduced from MD studies, located the competitive inhibitors **11** and **12** in proximity to the heme group in CYP2D2 and -2D6, it should be noted that this is not necessarily the case for all competitive inhibitors or all P450s. Binding to the substrate access channel may additionally be possible, as are multiple binding modes. To establish whether the former binding mode is a favorable one, however, requires accurate simulation of the opening and closing of the substrate access channel. This is currently not possible for homology models. In contrast to **11** and **12**, sparteine (**10**) was found to be unable to form a hydrogen bond with either residue 301 (an aspartate) or 216 (an aspartate or glutamate) in the active sites of CYP2D2 and -2D6. Instead, **10** contained an internal hydrogen bond (parts E and F of Figure 6). Because of the absence of specific interactions such as π-stacking and hydrogen bonds, the difference in IC_{50} value between CYP2D2 and -2D6 for **10** is likely to be due to differences in van der Waals interactions. Indeed, **10** showed close van der Waals contacts, especially with CYP2D2 residues Met304 and Ile374 (Figure 6E). Shielding of negatively charged residues may additionally play a role. In CYP2D2, Asp216 was found to adopt a conformation in which it formed a salt bridge with Lys243. In CYP2D6, Glu216 does not have a positively charged residue in the vicinity to counteract its negative charge.

In conclusion, the use of rabbit CYP2C5 as a new mammalian structural template for modeling human CYP2D6 has resulted in an improved homology model, which is stable during MD simulation and corroborates available data from metabolism, mutation, and spectroscopic studies. With the novel CYP2D6-derived rat CYP2D1−4 homology models, observed differences in IC_{50} values toward 11 CYP2D6 ligands could be rationalized. The electrostatic potential of the CYP2D1−4 and CYP2D6 active sites was found to dictate overall binding affinities toward ligands, whereas differences in IC_{50} values of individual ligands could be rationalized by differences in binding modes and active site residues. The latter notably included CYP2D6 residues 120, 216, 217, 301, 304, 374, and 483. CYP2D2 was found to be the most important rat isoform in terms of ligand binding. CYP2D2 was also the rat isoform, which resembled human CYP2D6 the most in ligand IC_{50} values. Nevertheless, CYP2D2 shared the lowest sequence identity in active site residues with CYP2D6 of

all rat CYP2D isoforms investigated. Sequence identity alone is therefore not a valid basis for data extrapolation.

Acknowledgment. The authors gratefully acknowledge the Center of Molecular Design, Division of Janssen Pharmaceutica (Vosselaar, Belgium), and Dr. Luc M. Koymans, in particular, for technical support and the use of their software. Ed Groot is gratefully acknowledged for his support regarding the competition studies.

References

(1) Bertz, R. J.; Granneman, G. R. Use of in vitro and in vivo data to estimate the likelihood of metabolic pharmacokinetic interactions. *Clin. Pharmacokinet.* **1997**, *32*, 210−258.
(2) Brockmoller, J.; Kirchheiner, J.; Meisel, C.; Roots, I. Pharmacogenetic diagnostics of cytochrome P450 polymorphisms in clinical drug development and in drug treatment. *Pharmacogenomics* **2000**, *1*, 125−151.
(3) Ingelman-Sundberg, M.; Oscarson, M.; McLellan, R. A. Polymorphic human cytochrome P450 enzymes: an opportunity for individualized drug treatment. *Trends Pharmacol. Sci.* **1999**, *20*, 342−349.
(4) See http://www.imm.ki.se/CYPalleles for more detailed information.
(5) Tucker, G. T. Clinical implications of genetic polymorphism in drug metabolism. *J. Pharm. Pharmacol.* **1994**, *46* (Suppl. 1), 417−424.
(6) Schulz-Utermoehl, T.; Bennett, A. J.; Ellis, S. W.; Tucker, G. T.; Boobis, A. R.; Edwards, R. J. Polymorphic debrisoquine 4-hydroxylase activity in the rat is due to differences in CYP2D2 expression. *Pharmacogenetics* **1999**, *9*, 357−366.
(7) Yamamoto, Y.; Tasaki, T.; Nakamura, A.; Iwata, H.; Kazusaka, A.; Gonzalez, F. J.; Fujita, S. Molecular basis of the Dark Agouti rat drug oxidation polymorphism: importance of CYP2D1 and CYP2D2. *Pharmacogenetics* **1998**, *8*, 73−82.
(8) Ellis, S. W.; Hayhurst, G. P.; Smith, G.; Lightfoot, T.; Wong, M. M.; Simula, A. P.; Ackland, M. J.; Sternberg, M. J.; Lennard, M. S.; Tucker, G. T.; et al. Evidence that aspartic acid 301 is a critical substrate-contact residue in the active site of cytochrome P450 2D6. *J. Biol. Chem.* **1995**, *270*, 29055−29058.
(9) Venhorst, J.; Onderwater, R. C.; Meerman, J. H.; Vermeulen, N. P. E.; Commandeur, J. N. M. Evaluation of a novel high-throughput assay for cytochrome P450 2D6 using 7-methoxy-4-(aminomethyl)-coumarin. *Eur. J. Pharm. Sci.* **2000**, *12*, 151−158.
(10) Crespi, C. L. Higher-throughput screening with human cytochromes P450. *Curr. Opin. Drug Discovery Dev.* **1999**, *2*, 15−19.
(11) Ekins, S.; de Groot, M. J.; Jones, J. P. Pharmacophore and three-dimensional quantitative structure activity relationship methods for modeling cytochrome p450 active sites. *Drug Metab. Dispos.* **2001**, *29*, 936−944.
(12) Gotoh, O. Substrate recognition sites in cytochrome P450 family 2 (CYP2) proteins inferred from comparative analyses of amino acid and coding nucleotide sequences. *J. Biol. Chem.* **1992**, *267*, 83−90.
(13) Kawashima, H.; Strobel, H. W. cDNA cloning of a novel rat brain cytochrome P450 belonging to the CYP2D subfamily. *Biochem. Biophys. Res. Commun.* **1995**, *209*, 535−540.
(14) Chow, T.; Hiroi, T.; Imaoka, S.; Chiba, K.; Funae, Y. Isoform-selective metabolism of mianserin by cytochrome P-450 2D. *Drug Metab. Dispos.* **1999**, *27*, 1200−1204.
(15) Chow, T.; Imaoka, S.; Hiroi, T.; Funae, Y. Developmental changes in the catalytic activity and expression of CYP2D isoforms in the rat liver. *Drug Metab. Dispos.* **1999**, *27*, 188−192.
(16) Wan, J.; Imaoka, S.; Chow, T.; Hiroi, T.; Yabusaki, Y.; Funae, Y. Expression of four rat CYP2D isoforms in *Saccharomyces cerevisiae* and their catalytic specificity. *Arch. Biochem. Biophys.* **1997**, *348*, 383−390.
(17) Onderwater, R. C.; Venhorst, J.; Commandeur, J. N. M.; Vermeulen, N. P. E. Design, synthesis, and characterization of 7-methoxy-4-(aminomethyl)coumarin as a novel and selective cytochrome P450 2D6 substrate suitable for high-throughput screening. *Chem. Res. Toxicol.* **1999**, *12*, 555−559.
(18) Williams, P. A.; Cosme, J.; Sridhar, V.; Johnson, E. F.; McRee, D. E. Mammalian microsomal cytochrome P450 monooxygenase: structural adaptations for membrane binding and functional diversity. *Mol. Cell* **2000**, *5*, 121−131.
(19) Venhorst, J.; Onderwater, R. C.; Meerman, J. H. N.; Commandeur, J. N. M.; Vermeulen, N. P. E. Influence of N-substitution of 7-methoxy-4-(aminomethyl)-coumarin on cytochrome P450 metabolism and selectivity. *Drug Metab. Dispos.* **2000**, *28*, 1524−1532.
(20) Penman, B. W.; Reece, J.; Smith, T.; Yang, C. S.; Gelboin, H. V.; Gonzalez, F. J.; Crespi, C. L. Characterization of a human cell line expressing high levels of cDNA-derived CYP2D6. *Pharmacogenetics* **1993**, *3*, 28−39.
(21) *Prism*, version 2.0; GraphPad Software Inc.: San Diego, CA, 1997.
(22) www.embl-heidelberg.de.
(23) www.rcsb.org/pdb.
(24) *InsightII*; Accelrys Inc.: San Diego, CA, 2000.
(25) Sali, A.; Blundell, T. L. Comparative protein modelling by satisfaction of spatial restraints. *J. Mol. Biol.* **1993**, *234*, 779−815.
(26) Laskowski, R.; MacArthur, M.; Moss, D.; Thornton, J. PROCHECK: a program to check the stereochemical quality of protein structures. *J. Appl. Crystallogr.* **1993**, *26*, 283−291.
(27) *Amber*, version 6.0; University of California: San Francisco, CA, 1999.
(28) Modi, S.; Paine, M. J.; Sutcliffe, M. J.; Lian, L. Y.; Primrose, W. U.; Wolf, C. R.; Roberts, G. C. A model for human cytochrome P450 2D6 based on homology modeling and NMR studies of substrate binding. *Biochemistry* **1996**, *35*, 4540−4550.
(29) *SACRD*; Center of Molecular Design (CMD), Division of Janssen Pharmaceutica: Vosselaar, Belgium, 1999.
(30) *Cambridge Structural Database* (CSD); Cambridge Crystallographic Data Centre (CCDC): Cambridge, U.K., 2000.
(31) *CONF*; Center of Molecular Design (CMD), Division of Janssen Pharmaceutica: Vosselaar, Belgium, 1998.
(32) Cieplak, P.; Cornell, W. D.; Bayly, C.; Kollman, P. A. Application of the multimolecule and multiconformational RESP methodology to biopolymers: Charge derivation for DNA, RNA, and proteins. *J. Comput. Chem.* **1995**, *16*, 1357−1377.
(33) *GAMESS US*; Ames Laboratory, Iowa State University: Ames, Iowa, 2000.
(34) Bayly, C. I.; Cieplak, P.; Cornell, W. D.; Kollman, P. A. A well-behaved electrostatic potential based method using charge restraints for deriving atomic charges: the RESP model. *J. Phys. Chem.* **1993**, *97*, 10269−10280.
(35) Cornell, W. D.; Cieplak, P.; Bayly, C. I.; Kollman, P. A. Application of RESP charges to calculate conformational energies, hydrogen bond energies, and free energies of solvation. *J. Am. Chem. Soc.* **1993**, *115*, 9620−9631.
(36) Gilson, M. K.; Honig, B. H. Calculation of electrostatic potentials in an enzyme active site. *Nature* **1987**, *330*, 84−86.
(37) Gilson, M. K.; Honig, B. Calculation of the total electrostatic energy of a macromolecular system: solvation energies, binding energies, and conformational analysis. *Proteins* **1988**, *4*, 7−18.
(38) Lightfoot, T.; Ellis, S. W.; Mahling, J.; Ackland, M. J.; Blaney, F. E.; Bijloo, G. J.; De Groot, M. J.; Vermeulen, N. P.; Blackburn, G. M.; Lennard, M. S.; Tucker, G. T. Regioselective hydroxylation of debrisoquine by cytochrome P4502D6: implications for active site modelling. *Xenobiotica* **2000**, *30*, 219−233.
(39) Schneider, F.; Fischer, P.; Ebner, T.; Meese, C. O. Conformation of the CYP2D6 model substrate sparteine under physiological conditions. *Bioorg. Med. Chem. Lett.* **1993**, *3*, 1667−1670.
(40) Ebner, T.; Meese, C. O.; Fischer, P.; Eichelbaum, M. A nuclear magnetic resonance study of sparteine delta metabolite structure. *Drug Metab. Dispos.* **1991**, *19*, 955−959.
(41) Hosea, N. A.; Miller, G. P.; Guengerich, F. P. Elucidation of distinct ligand binding sites for cytochrome P450 3A4. *Biochemistry* **2000**, *39*, 5929−5939.
(42) Ueng, Y. F.; Kuwabara, T.; Chun, Y. J.; Guengerich, F. P. Cooperativity in oxidations catalyzed by cytochrome P450 3A4. *Biochemistry* **1997**, *36*, 370−381.
(43) Koymans, L. M.; Vermeulen, N. P.; Baarslag, A.; Donne-Op den Kelder, G. M. A preliminary 3D model for cytochrome P450 2D6 constructed by homology model building. *J. Comput.-Aided Mol. Des.* **1993**, *7*, 281−289.
(44) Lewis, D. F.; Eddershaw, P. J.; Goldfarb, P. S.; Tarbit, M. H. Molecular modelling of cytochrome P4502D6 (CYP2D6) based on an alignment with CYP102: structural studies on specific CYP2D6 substrate metabolism. *Xenobiotica* **1997**, *27*, 319−339.
(45) de Groot, M. J.; Vermeulen, N. P.; Kramer, J. D.; van Acker, F. A.; Donne-Op den Kelder, G. M. A three-dimensional protein model for human cytochrome P450 2D6 based on the crystal structures of P450 101, P450 102, and P450 108. *Chem. Res. Toxicol.* **1996**, *9*, 1079−1091.
(46) de Groot, M. J.; Ackland, M. J.; Horne, V. A.; Alex, A. A.; Jones, B. C. Novel approach to predicting P450-mediated drug metabolism: development of a combined protein and pharmacophore model for CYP2D6. *J. Med. Chem.* **1999**, *42*, 1515−1524.

(47) De Rienzo, F.; Fanelli, F.; Menziani, M. C.; De Benedetti, P. G. Theoretical investigation of substrate specificity for cytochromes P450 IA2, P450 IID6 and P450 IIIA4. *J. Comput.-Aided Mol. Des.* **2000**, *14*, 93−116.
(48) Ellis, S. W.; Harlow, J.; Chowdry, J.; Tucker, G. T. Active-site residues of CYP2D6—Fact and fiction. Presented at the 12th IGH International Conference on Cytochrome P450, 2001; Poster Abstract 70.
(49) Hanna, I. H.; Kim, M. S.; Guengerich, F. P. Heterologous expression of cytochrome P450 2D6 mutants, electron transfer, and catalysis of bufuralol hydroxylation: the role of aspartate 301 in structural integrity. *Arch. Biochem. Biophys.* **2001**, *393*, 255−261.
(50) Ellis, S. W.; Rowland, K.; Ackland, M. J.; Rekka, E.; Simula, A. P.; Lennard, M. S.; Wolf, C. R.; Tucker, G. T. Influence of amino acid residue 374 of cytochrome P-450 2D6 (CYP2D6) on the regio- and enantio-selective metabolism of metoprolol. *Biochem. J.* **1996**, *316*, 647−654.
(51) Smith, G.; Modi, S.; Pillai, I.; Lian, L. Y.; Sutcliffe, M. J.; Pritchard, M. P.; Friedberg, T.; Roberts, G. C.; Wolf, C. R. Determinants of the substrate specificity of human cytochrome P-450 CYP2D6: design and construction of a mutant with testosterone hydroxylase activity. *Biochem. J.* **1998**, *331*, 783−792.
(52) Ellis, S. W.; Hayhurst, G. P.; Lightfoot, T.; Smith, G.; Harlow, J.; Rowland-Yeo, K.; Larsson, C.; Mahling, J.; Lim, C. K.; Wolf, C. R.; Blackburn, M. G.; Lennard, M. S.; Tucker, G. T. Evidence that serine 304 is not a key ligand-binding residue in the active site of cytochrome P450 2D6. *Biochem. J.* **2000**, *345* (Part 3), 565−571.
(53) Ridderstrom, M.; Zamora, I.; Fjellstrom, O.; Andersson, T. B. Analysis of selective regions in the active sites of human cytochromes P450, 2C8, 2C9, 2C18, and 2C19 homology models using GRID/CPCA. *J. Med. Chem.* **2001**, *44*, 4072−4081.
(54) Wade, R. C.; Gabdoulline, R. R.; Ludemann, S. K.; Lounnas, V. Electrostatic steering and ionic tethering in enzyme-ligand binding: insights from simulations. *Proc. Natl. Acad. Sci. U.S.A.* **1998**, *95*, 5942−5949.
(55) Cosme, J.; Johnson, E. F. Engineering microsomal cytochrome P450 2C5 to be a soluble, monomeric enzyme. Mutations that alter aggregation, phospholipid dependence of catalysis, and membrane binding. *J. Biol. Chem.* **2000**, *275*, 2545−2553.
(56) Hasemann, C. A.; Kurumbail, R. G.; Boddupalli, S. S.; Peterson, J. A.; Deisenhofer, J. Structure and function of cytochromes P450: a comparative analysis of three crystal structures. *Structure* **1995**, *3*, 41−62.

JM0209578